

# Nanometric leveling and optical selectivity enhancement of black nickel electrodeposited on C81100 high conductive copper

R. L. P. Teixeira, R. A. Simão, B. Coelho and A. C. Oliveira

**Abstract**— A black nickel solar absorber film with high absorptance in the solar spectrum ( $\alpha$ ) and low thermal emittance ( $\epsilon$ ) was electrodeposited on nickel films produced by the Watts solution on nanometric leveled C81100 copper. This high conductivity C81100 copper substrate was nanometrically leveled by electrochemical polishing to minimize textural surface effects as well as light trapping and optical losses. The nanometric leveled black nickel layer presented a thickness of  $(2.9 \pm 0.1) \mu\text{m}$  and a selectivity ( $\alpha/\epsilon$ ) of 11, against a selectivity ( $\alpha/\epsilon$ ) of 8.9 for the non structured condition. The nanometric leveled black nickel presented a higher concentrated statistical dispersion of grain range size and lower nanometric RMS, a diameter deviation of 17 nm against 42 nm for the non structured condition. AFM and optical results confirmed that the nanometric size of black nickel grains and their grain size standard deviation are decisive factors to decrease the emittance and increase the final selectivity.

**Keywords**— Ceramic-matrix composites (CMCs), atomic force microscopy, infrared (IR) spectroscopy, scanning electron microscopy (SEM).

## I. INTRODUCTION

Nanostructured materials are a new class of engineering materials with specific properties and structural length between 1 and 100 nm, which can be produced by a variety of different methods. Nanometric and submicronmetric systems are being studied as actuators, sensors, micromotors, and frictionless gears using magnetic materials, in fabrication of nanostructured magnetic material and high performance cermet solar selective surfaces for solar energy applications, such as a solar absorber [1, 2].

Renewable energies from natural resources such as sunlight, wind, rain, tides, and geothermal heat represent answers to decrease climate changes due to harmful pollutant emissions from conventional energy sources (petroleum, coal and others). Moreover, solar thermal energy has probably the greatest potential, compared to other renewable energy resources, because the energy coming from the sun is the most powerful, cleanest and stable source (a solar energy per  $\text{m}^2$  per day has 7 kWh energy content). The amount of sunlight striking the Earth's atmosphere continuously is  $1.75 \times 10^5 \text{ TW}$ , with 60% passing through the atmospheric cloud cover, so that  $1.05 \times 10^5 \text{ TW}$  of energy reaches the Earth's surface continuously. If the irradiance on only 1% of the Earth's

surface could be converted into electric energy with a 10% efficiency, it would provide  $10^5 \text{ TW}$  of energy, whereas the total global energy needs for 2050 are projected to be only about 25–30 TW. A solar collector is an apparatus that collects the sunlight energy then alters this energy into a more usable or storable energy form. The present state of the art solar energy technologies is such that solar-cell efficiencies have reached over 20% and solar thermal systems 40 % – 60 % are efficient. Solar PV panels have come down in cost from about \$30 per W to about \$3 per W in the last three decades. At \$3 per W panel cost, the overall system cost is around \$6 per W, which is still too high to compete with other resources on the electricity grid. However, there are many off-grid applications where solar PV is already cost-effective, especially with governmental incentives, such as feed-in laws [3-7].

Absorber coatings such as black nickel, black chromium and black cobalt have been applied as fairly efficient solar collector surfaces. Several techniques, such as vacuum techniques (sputtering, electron beam, chemical vapor deposition, etc.), sol-gel, electroless deposition (catalytic reduction process) are currently used to produce solar absorber surfaces. However, the desired characteristics of the solar absorber coating may be better controlled by direct electrodeposition such as their nanostructuration [8]. The synthesis of nanomaterials requires an atomistic deposition process and extreme control over the deposition. Despite the fact that vacuum techniques have been used almost exclusively to produce these materials, electrochemical deposition, that is also an atomic deposition process, can be used to synthesize nanocomposites, and has generated a great deal of interest in recent years. The electrodeposition advantages against vacuum techniques are basically the following [6, 9]:

- a. Rapidity;
- b. Low cost;
- c. Free from porosity;
- d. High purity;
- e. Industrial applicability;
- f. Potential to overcome shape limitations or allowing the production of free-standing parts with complex shapes;
- g. Higher deposition rates;
- h. Ability to produce coatings on widely differing substrates;
- i. Ability to produce structural features with sizes ranging

from nm to  $\mu\text{m}$ ;

- j. Easy to control alloy composition;
- k. Ability to produce compositions unattainable by other techniques;
- l. The possibility of forming of simple low-cost multilayers in many different systems, e.g. Cu/Ni, Ni/Ni-P etc;
- m. No post-deposition treatment.

Advantages of copper substrate for selective coatings in solar applications are [10]:

- a. Longer life or durability in piping systems suitable for heating fluids up to 85 °C;
- b. Higher thermal and electrical conductivity (lower energy losses) and low maintenance costs.
- c. Copper tubes are the standard plumbing material for potable water and heating systems in most European countries;
- d. Other choices are chemical affinity and well known processes and reactions [11].

A thin layer of nickel is plated to copper substrates to improve wear resistance and to prevent the copper oxidation, besides promoting better black nickel adhesion [11]. Solar absorptance and thermal emittance are the two main parameters for characterizing the spectrally selective nature of solar absorbing coatings at specific wavelengths' ranges. The solar absorptance, is the weighted fraction between absorbed radiation and incoming solar radiation (in the solar wavelength range) and can be calculated by 100 less the reflectance (in %). The emittance is described as the ability of a surface to radiate thermal or infrared radiation (mIR, thermal or mid infrared wavelength range) and can be calculated by 100 minus the reflectance (in %). Selectivity is the comparative fraction between absorptance and emittance. The best selective absorbers present selectivity values over 10, denoting higher sunlight energy absorption and lower thermal energy losses [12].

Mid-temperature absorber coatings are coatings that can be useful to applications below 200 °C. Mid-temperature absorber coatings are summarized in Table I, with comparative results of the selectivity ratio ( $\alpha/\epsilon$ ), with the emittance ( $\epsilon$ ) reported at 100 °C (emittance measurements made by the Gier-Dunkle instrument are measured at room temperature) [2].

A black nickel Cermet solar mid-temperature absorber can be applied onto various metal substrates using an electroplating technique. Black nickel Cermet electrodeposits are composed of a nickel-rich co-deposit of nickel and zinc that is formed from the reduction of thiocyanate and leads to the incorporation of sulfide in the deposit at about 1 to 2 mA/cm<sup>2</sup> [13]. The mechanism of dark blackening was attributed to the deposition of these sulfide particles in the Ni-Zn alloy [1]. This sulfide ceramic layer with metallic inclusions (or cermet) acts as a selective surface. The presence of reflective particles at the infrared spectrum inside the ceramic bulk may increase the efficiency of solar energy conversion into thermal energy in thin films of metal-

dielectric composites, like nanoporous nickel oxide (NiO) with Ni inclusions [14]. Different groups have modified the electrodeposition bath and process to produce coatings with selectivity ( $\alpha/\epsilon$ ) of 0.88-0.96 / 0.03-0.10, for temperatures below 200 °C. Black nickel can degrade in humid environments when exposed to temperatures of 200 °C and is therefore not applicable for concentrating solar power applications (CSP). Kennedy reported that by incorporating topological micrometric roughness into the Maxorb's black nickel, they enhanced the solar selectivity ( $\alpha/\epsilon$ ) = 12.1 (0.97/0.08) of their black nickel together texturing effects (roughness coherent with sunlight wavelengths increases absorptance due to the topographic light trapping). Black Crystal™ or Black Forest™, are non-oxidized metallic Ni-Sn alloy solar-selective coatings on a copper substrate. Nearly all other black nickel solar-selective coatings contain nickel oxides. Their high solar-absorbing characteristics, ( $\alpha/\epsilon$  = 0.92-0.98/0.08-0.25) with a thermal stability up to 300 °C, are a result of the micro-surface light-trapping morphology. This coating is produced by combining two processes: the electrodeposition of the crystallographic metallic alloy and applying a sol-gel overcoat. It has been developed jointly by Energy Laboratories, Inc. (ELI) in Jacksonville, Florida, and Sandia National Laboratories. This work is being done under a cooperative research and development agreement (CRADA) and is funded by both the U.S. Department of Energy (DOE) CSP and Solar Buildings Programs. The black nickel is reported by Kennedy as not appropriate for deployment in evacuated tube-type systems [2].

Black chrome (Cr-Cr<sub>2</sub>O<sub>3</sub>), an electrodeposited Cr-Cr<sub>2</sub>O<sub>3</sub> cermet on Ni, Fe, Cu, stainless-steel substrates, has a selectivity ( $\alpha/\epsilon$ ) of 0.97/0.09 for temperatures below 300 °C, being produced by MTI on Ni-plated Cu in the United States, by ChromeCoat of Denmark on copper, and on stainless-steel by Energie Solaire in Switzerland. Kennedy reports that a layer of Ni between the substrate and black chrome coating gives better stability up to 400 °C. Oxidation of the metallic Cr and densification of the crystallites primarily cause the degradation of the selective coating, and high temperatures products, atomic nickel diffusion from the substrate and consequently optical degradation [2]. Black chrome solar selective films can be modified by mixing molybdenum, up to 20% of the chromium content. Absorptance is stable for a Mo/Cr ratio of 0.6% at a value of 0.95 for 146 hours at temperatures up to 425 °C in air. Black chrome is also reported by Kennedy as not appropriate for deployment in evacuated tube-type systems [2].

Stable nickel (Ni)-pigmented alumina (Al<sub>2</sub>O<sub>3</sub>) Cermet selective surface coatings on aluminum substrates, intended for flat-plate collectors, are widely reported, with  $\alpha/\epsilon$  (100 °C) of 0.85-0.97/0.08-0.21 for 300 °C < T < 500 °C, and are commercially produced by TeknoTerm Energi in Sweden and Showa in Japan. They are made by the phosphoric anodic anodization of aluminum whose pores are impregnated with Ni, but other metals such as V, Cr, Co, Cu, Mo, Ag, Si, and W can be used [2]. The lifetime of this selective surface is shortened by exposure to high temperature, humidity, and

atmospheric pollution such as sulfur dioxide and abrasion also. The addition of a mechanically stable transparent coating reduces the degradation due to abrasion, high temperature, weathering, and chemical attacks. The nickel-pigmented alumina is reported by Kennedy as unlikely to be suitable for CSP applications [2].

For nucleation in electroplating, equation (1) describes Avrami's relationship of the current ( $i$ ) versus time ( $t$ ) that can be used for instantaneous nucleation under steady-state. This equation can be applied for a black nickel absorber and proves that the electric current is proportional to the square root of time, conducting to instantaneous nucleation [8].

$$i = z \cdot F \cdot D^{1/2} \cdot N \cdot K \cdot t^{1/2} \quad (1)$$

For black nickel electrochemical reactions, in the beginning of electrolysis, nickel, nickel-zinc alloy and/or zinc are deposited and hydrogen gas is released from the surface. Nonetheless, hydrogen gas releasing decreases during the process due to over voltage of the metals. The increase in alkalinity at the metal solution interface results on the formation of nickel and zinc complex ions, interfering on the metallic cationic reduction and deposition of thiocyanate. The deposition of black nickel sulfate ions and thiocyanate on the metal surface lowers the over voltage of hydrogen to nearly the same value as in the beginning of the process, and then the cycle is repeated [15].

The optical characteristics of nanostructured and non nanostructured electrodeposited black nickel were compared by atomic force microscopy, scanning electron microscopy and optical UV-VIS-nIR and mIR spectrophotometry for understanding the nanostructuration effect in their optical characteristics.

## II. EXPERIMENTS

The proposed absorber samples were processed for black nickel coating by a standard sulphamate electrolytic solution using the following sequence of operations:

1) Nanometric leveling of metallic substrates: mechanical unidirectional polishing (P1200) of C81100 copper substrates ( $1 \times 1 \text{ cm}^2$ ) [16]; copper electrochemical polishing in 85 %v/v  $\text{H}_3\text{PO}_4$  a 1750 mV (DC) for 180 seconds ( $3 \times 60$  seconds), only for nanostructured sample [17];

2) Electrodeposition of the solar absorber coating: the nickel underlayer deposition by nickel Watts bath, 2 mA/cm<sup>2</sup> for 5 minutes; the black nickel absorber coating by Fishlock bath, 0.2 mA/cm<sup>2</sup> for 15 minutes [11], on nanostructured and non structured samples.

To plate the black nickel samples it was used a bath composed of nickel sulfate, nickel ammonium sulfate, zinc sulfate, and sodium thiocyanate [11]. All plating baths and reactants were made from Vetec chemicals (Vetec Química Fina Ltda) and Milli-Q™ water.

Scanning Electron Microscopy (SEM) and Energy Dispersive X-ray (EDS) spectroscopy of the black nickel samples were performed using JEOL JSM-6460 LV and EDX

Noran in 200 kV (EDS), respectively. Back scattered electron imaging, qualitative X-ray analysis, and cross-section images were obtained.

Ultraviolet-visible- near infrared spectroscopy (UV-VIS-NIR absorption patterns) of the black nickel samples were obtained using a Perkin Elmer™ Lambda 950 spectrophotometer with wavelength of 175 nm at 2500 nm, Labsphere's Spectralon® reflectance material were used as standard sample for calibration (reflectance > 95%). Mid infrared (MIR or thermal infrared, wavelength of 3 to 8  $\mu\text{m}$ ) of the black nickel samples were estimated with Perkin Elmer Spectrum GX using as reference a polished nickel plate (with reflectance > 95%).

AFM images of the black nickel samples have been recorded using intermittent contact mode operation on a JPK™ atomic force microscope (JPK Instruments-Nanotechnology for Life Science) under ambient condition, relative humidity between 45% and 55%. Micromasch™ rectangular cantilever NSC16/AIBS has been employed to obtain topography and phase contrast images. Magnetic force microscopy (MFM) images of the black nickel surface were obtained by using the same tips coated with Co-Cr. Image resolution has been set to 512 X 512 points.

## III. RESULTS AND DISCUSSION

### III.1. MORPHOLOGY: ELECTRON MICROSCOPY WITH MICROANALYSIS ENERGY DISPERSIVE X-RAY SPECTROSCOPY (SEM WITH EDS)

The film thickness was evaluated using cross section images from photomicrography of the nickel Watts (Fig.1) and the black nickel [18]. The nickel Watts system (nickel Watts/copper film or Ni/Cu) presented a layer of thickness around  $(1.4 \pm 0.1) \mu\text{m}$  from Fig. 1(b), and the black nickel layer presented a thickness of  $(2.9 \pm 0.1) \mu\text{m}$  [18]. The nickel Watts underlayer EDS spectrum in Fig. 1(b) detected mainly nickel and copper atoms. The black nickel layer EDS spectrum in Fig. 2(b) detected mainly zinc, nickel, sulfur and carbon atoms. The discontinuities of the nanostructured condition in Fig. 2(a) can be explained by nickel tensional surface behavior. A smooth surface is a necessary condition to produce creeping (belt slip) [19] and grains; on the other hand, the walls in the non structured sample come from peaks of polishing.

The EDS surface analysis for black nickel nanostructured and non structured coating, Fig. 3(b), showed the presence of zinc, nickel, sulfur and carbon in the black nickel layer. Fig. 3(a) shows that the black nickel nanostructured surface is very smooth with some discontinuities. Contrarily, the non nanostructured black nickel, has higher peaks or valleys from the mechanical unidirectional P1200 polishing. The non nanostructured black nickel presented a stronger EDS signal for nickel (Fig. 3(b)) that was indicative of higher deposition rate than for nanostructured black nickel. The intense copper signals in Fig. 3(b) for non structured black nickel were due to the higher peaks than in nanostructured black nickel. The

presence of higher peaks increases the current density, modifying local electrodeposition [20, 21]. However, the black nickel nanostructured stressional behavior did not affect the adhesion of black nickel coating.

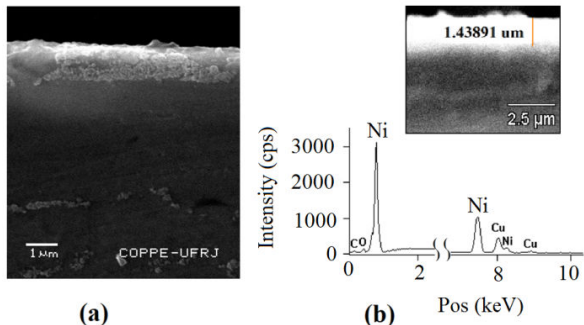


Fig.1. Nickel Watts cross-section image: (a) SEM: 10 000  $\times$  and (b) EDS.

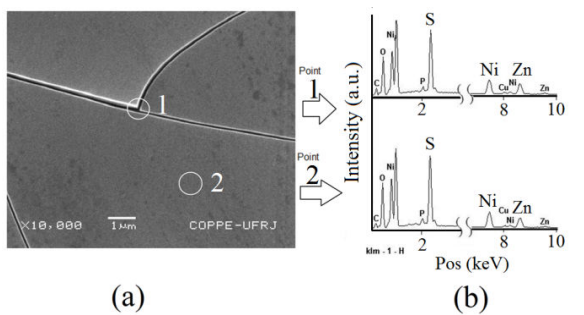


Fig.2. Black nickel surface: (a) SEM: 10 000  $\times$  and (b) EDS.

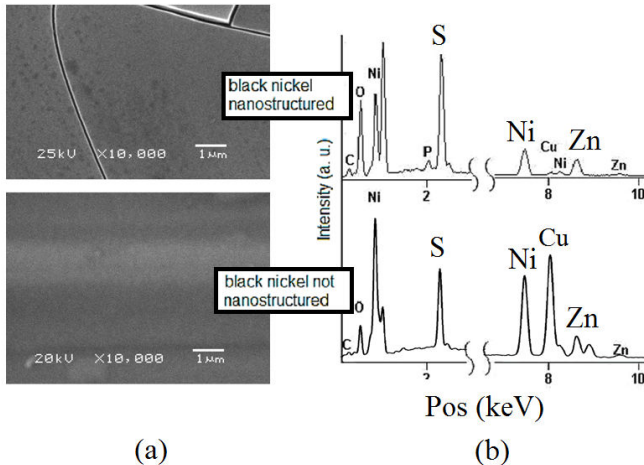


Fig.3. Black nickel coating: (a) SEM: 10 000  $\times$  and (b) EDS.

### III.2. OPTICAL ANALYSIS – SPECTROMETRY UV, VIS, NIR AND MIR

Solar absorptance and thermal emittance are the main parameters to compare the optical properties of solar absorbing coatings. Fig. 4(a) shows reflectance (%) versus wavelength ( $\mu\text{m}$ ) of the nanostructured black nickel, the non structured black nickel and an ideal solar selective surface. Fig 4(a) shows that all black nickel cermet conditions

(nanostructured and non nanostructured) behave close to an ideal selective material, with the best values for the black nickel as compared to the values listed in Table I.

Table I. Mid-temperature of some black selective surfaces [2].

Material	Fabrication Method	Absorptance ( $\alpha$ )	Emittance ( $\epsilon$ )	Commercial Product
Black nickel NiS-ZnS	Electrodeposition	0.96 - 0.98	0.03 - 0.10	Maxorb
Black nickel Ni-Sn	Electrodeposition / Sol-gel	0.92 - 0.98	0.08 - 0.25	Black Crystal
Black copper BiCu-Cu <sub>2</sub> O:Cu	Electrodeposition / Sol-gel	0.97 - 0.98	0.02	
Black chrome Cr-Cr <sub>2</sub> O <sub>3</sub>	Electrodeposition	0.97	0.09	MTI ChromeCoat Energie Solaire
Black chrome	Electrodeposition	0.95	< 0.30	MTI ChromeCoat Energie Solaire
Ni-NiO <sub>x</sub>	reactive sputtering	0.96	0.10	Sunstrip
Ni pigmented Al <sub>2</sub> O <sub>3</sub>	Anodization	0.85 - 0.97	0.08 - 0.21	TeknoTerm Energi Showa

The ideal selective surface in Fig. 4(a) has zero reflectance (absorptance ( $\alpha$ ) = 1 – reflectance = 1 or 100 %) between 0.3 and 2.5  $\mu\text{m}$  and unity reflectance (emittance ( $\epsilon$ ) = 1 – reflectance = 0 or 0%) in the infrared region, between 2.5 and 25  $\mu\text{m}$  [2]. Fig. 4(a) presents the reflectance of the surface at different wavelengths. In Fig. 4(a), the nanostructured condition presents a selectivity ( $\alpha/\epsilon$ ) = 11.0 (0.977 / 0.089), for wavelengths between  $\lambda$  = 300 - 2500 nm, and the non nanostructured a selectivity ( $\alpha/\epsilon$ ) = 8.9 (0.964 / 0.110) for  $\lambda$  = 2500 - 25000 nm. Fig. 4(b) bar graph was used to show how optical properties absorptance ( $\alpha$ ) and emittance ( $\epsilon$ ) change over nanostructuration conditions. Fig. 4(b) bar graph displays data against cumulative properties, with the properties in each nanostructuration condition combined and displayed as subgroups. In Fig. 4(b), the absorptance for both structuration conditions for  $\lambda$  = 300 - 2500 nm shows a similar relative weight between both conditions of nanostructuration, thus the absorptances of 96.4 % of the non nanostructured condition and 97.7 % of the nanostructured condition are equivalent. The emittance curves for  $\lambda$  = 2500 - 25000 nm (300 K) present different behavior between nanostructured and non nanostructured conditions (Fig. 4(a) and bar graph, Fig. 4(b)): emittance presents a higher influence than absorptance in the increasing of selectivity with nanostructuration. The emittance decreases from 11 % in non nanostructured condition to 8.9 % in nanostructured condition - Fig. 4(b). Therefore, nanostructuration increases the selectivity from 8.8 in non nanostructured condition to 11 % in nanostructured condition, mainly due to the decrease in emittance.

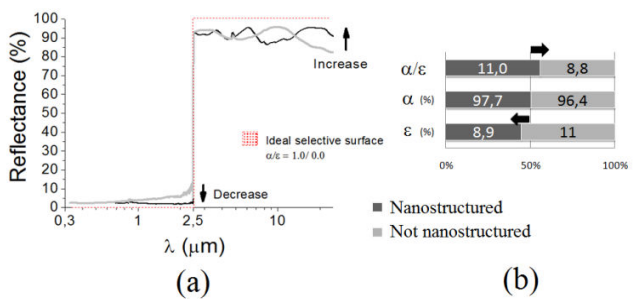


Fig.4. (a) Reflectance of black nickel coatings ( $\lambda = 0.3\text{-}25 \mu\text{m}$ ) and (b) stack bar graph of black nickel coatings optical properties.

### III.3 Topography and Physical Analysis: Atomic Force Microscopy and Magnetic Force Microscopy

AFM micrometric image of samples - Fig. 5(a) and Fig. 5(b) - compare the P1200 polished and electropolished samples and show the nanostructuration effects on the surface of the electropolished copper plates via a multistep method. The JPK™ root mean square roughness (RMS) deviation has decreased from 114.6 nm (submicrometric) in the mechanical polished surface to 24.5 nm in the electropolished surface. Also, the JPK™ maximum peak height is reduced from  $(504.1 \pm 0.1)$  nm (mechanical polished surface) to  $(39.8 \pm 0.1)$  nm (electropolished surface). Furthermore, better statistical height dispersion in the electropolished copper surface was registered. Thus, JPK™ AFM analysis results show that copper bulk was nanometrically leveled.

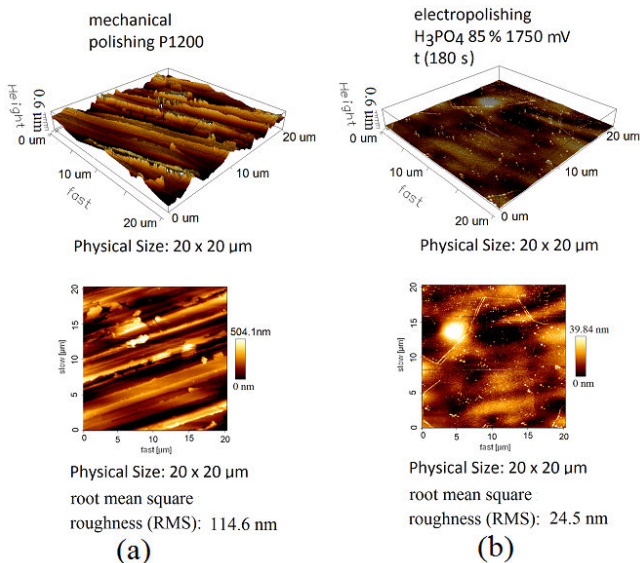


Fig.5. AFM  $20 \times 20 \mu\text{m}$  images and statistical JPK™ roughness, (a) copper mechanical P1200 polished and (b) copper electropolished.

To confirm the dimensions of the black nickel coating grain size, phase contrast and topography scanning images were performed with SPIP™ image analyses. Fig. 6(c) and 6(f) AFM SPIP™ parameters of the black nickel absorber from

AFM images are presented. Fig. 6(a) and Fig 6(b)(not nanostructured condition) indicate the presence of smaller and some periodic submicrometric grains. Analysis is presented in Fig. 6(c). AFM images in Fig. 6(d) and Fig 6(e) (nanostructured condition) indicates the presence of smaller and some periodic nanometric that confirms the black nickel nanostructuration, Fig. 6(f). In Fig. 6(c) and 6(f), RMS and maximum height of the nanostructured and non nanostructured topography are lower than sunlight wavelengths and therefore, out of the surface texturing condition reported by Kennedy [2]; this consideration means that sunlight absorbing effect in the surface is similar. Fig. 4(b) showed similar absorptance for both conditions too. However, in Fig. 6(c) and 6(f), the nanostructured black nickel presented a higher concentrated grain range size and lower nanometric RMS, a roughness deviation of 17 nm against 42 nm for the non structured condition, as well as better SEM morphological isotropy [22] as observed in Fig. 3.

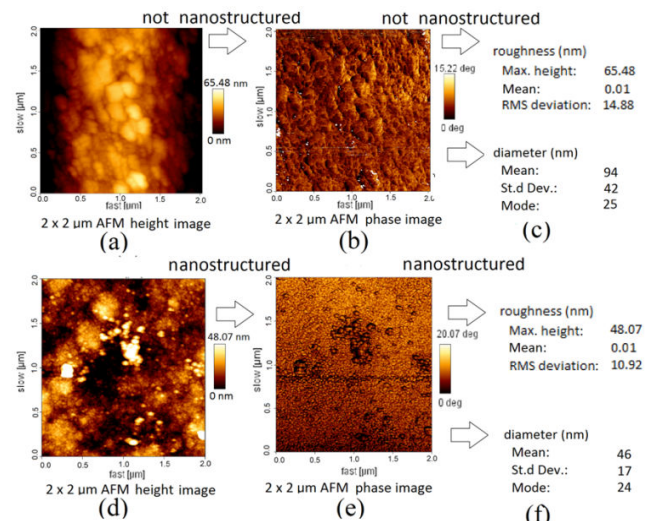


Fig.6. AFM  $2 \times 2 \mu\text{m}$  images: nanostructured black nickel (a) topography, (b) phase contrast image, and (c) SPIP™ diameter grain size and JPK™ roughness; nanostructured black nickel cermet (d) topography and (e) phase contrast image and (f) SPIP™ diameter grain size and JPK™ roughness.

The JPK™ AFM topography image presents a maximum height of 65.48 nm for the non nanostructured condition in figures 6(a) and 6(c) while the maximum height is 48.07 nm for nanostructured condition in figures 6(d) and 6(e). The JPK™ AFM phase contrast presents a mean particle size roughness of  $(94 \pm 42)$  nm and a mode of 25 nm for non nanostructured black nickel in figures 6(b) and 6(c). For the nanostructured condition to the mean particle size roughness is  $(46 \pm 17)$  nm with a mode of 24 nm in figures 6(d) and 6(e). The topography and grain size results in figures 6(c) and 6(f) confirm the nanostructuration of the black nickel absorber coating (nanometric statistical dispersion of the topography and contrast phase of the black nickel grains) in both conditions, but the nanostructured condition has lower values

of grain size (diameter) as shown in Fig. 6(c) and 6(f).

There is an indicative correlation in Fig 7 between optical properties, roughness and grain size, when comparing results from the atomic force microscopy (AFM) with the optical spectrophotometry (figures 4(b)). The results for surface roughness of black nickel shown in figures 6(c), 6(f) and 7 present the same JPK™ mean roughness of 0.01 nm, and a root mean square (RMS) roughness of 14.88 nm in non structured condition and 10.92 nm in nanostructured condition; this decrease in RMS of nanostructured condition coincides with a small improvement of absorptance - figures 4(a), 4(b) and 7. However, the grain size difference could justify the increase in selectivity of nanostructured condition - figures 4(b) and 7 - due to the decrease in emittance for the nanostructured condition. The lower grain sizes increase the specific surface area in nanostructured condition and improve selectivity, considering equivalent absorptance conditions - Fig. 4(b) and Fig. 7.

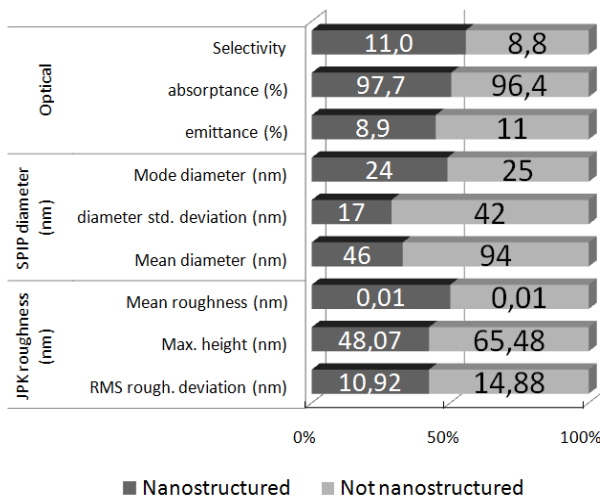


Fig.7. Stack bar graph of optical properties, diameter grain size and roughness of black nickel coatings.

The mean size of metallic nickel grains was indirectly interpreted, associating the MFM image and the grain size analyses to the black nickel absorber [23]. In figures 8(a) and 8(d), JPK™ AFM results shows that black nickel is topographically nanostructured. Furthermore, in Fig. 8(c), a magnetic domain structure is presented by the MFM trace lock-in phase image. This image presents a SPIP™ AFM estimate mean diameter particle size of  $(31 \pm 16)$  nm and mode diameter particle size of 6 nm, Fig. 8(d). These nanometric particles were attributed to the ferromagnetic metallic nickel phase, as nickel is found in EDS analysis - Fig. 3(b). Fig. 8(c) shows a one-domain structure, “round-up” points nanometrically dispersed lock-in phase image as observed by Xiansong Liu [24]. Lock-in phase at lifting in 35 nm of the surface correspond to an indicative presence of ferromagnetic metallic nickel in the black nickel cermet matrix NiS-ZnS thus metallic nickel particles are nanometrically dispersed on black nickel surface, nickel

particles present a nanometric statistical dispersion. The metallic nickel nanometric statistical dispersion (st. deviation) on black nickel surface indicates that black nickel is also chemically nanostructured surface [25, 26]. Therefore, the black nickel cermet behavior corresponds to a strong absorption in the solar region, and a high inner reflection in the IR region, due to inter-band transitions related to NiS-ZnS in combination with small metal particles. The dispersion of the metallic nickel particle in the nanostructured black nickel film can be related to the homogeneity of charges on the electrode surface during deposition inducing more nucleation sites for the metallic particles and decreasing thus their size.

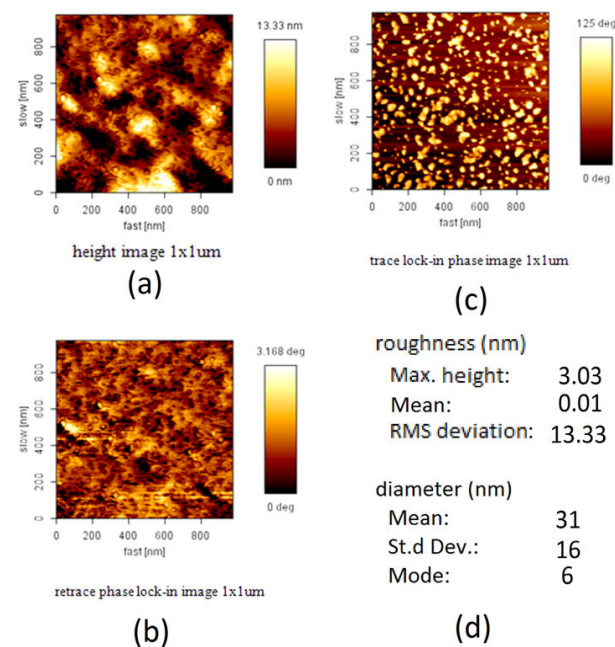


Fig.8. MFM images with lifting in of 35 nm with JPK™ roughness and AFM SPIP™ diameters. (a) MFM images  $1 \times 1 \mu\text{m}$  of the height (topography profile), (b) retrace lock-in phase image (c) trace lock-in phase image and (d) SPIP™ diameter grain size and JPK™ roughness of the black nickel coating nanostructured coating.

#### IV. CONCLUSIONS

Surface analysis by EDS for black nickel nanostructured and non structured coating, showed the presence of zinc, nickel, sulfur and carbon in the black nickel layer. The black nickel nanostructured surface is very smooth, with some discontinuities due to nickel tensional surface behavior, and the non nanostructured black nickel presented higher peaks or valleys from the mechanical unidirectional P1200 polishing. The black nickel nanostructured stressional behavior did not affect the adhesion of black nickel coating.

AFM images confirmed the success of the surface nanometric leveling to produce a nanostructuration of the black nickel coating topography as well as on grain size. The copper bulk RMS roughness deviation has decreased from 114.6 nm (submicrometric), in the mechanically P1200 polished surface, to 24.5 nm in the electropolished surface

(copper nanostructured condition), and the black nickel maximum height of 65.48 nm from the non nanostructured condition to 48.07 nm of the nanostructured condition, with a mean particle size of  $(46 \pm 17)$  nm mean roughness and a mode of 24 nm for the not nanostructured compared to  $(94 \pm 42)$  nm of the nanostructured condition. These results of topography and grain size for nanostructured condition confirm the nanostructuration of the black nickel absorber coating (nanometric statistical dispersion of the topography and contrast phase of black nickel grains).

MFM images SPIP™ analysis detected nanometric standard deviation of the ferromagnetic particles that was attributed to the presence of nanometrically dispersed ferromagnetic phase. These particles dispersion indicates a chemical structuration of nickel particles on the black nickel surface for the nanostructured condition. The presence of metallic nickel particles affected the optical proprieties of black nickel nanostructured condition mainly due to high reflectance in infrared wavelength.

The results of solar absorptance, thermal emittance and selectivity indicate that the optical parameters of the absorber samples are affected by nanostructuration of the black nickel. The black nickel nanostructured sample presented a higher selectivity of 11, against 8.9 of the non structured condition. AFM and optical results confirmed that the nanometric size of black nickel grains and their grain size standard deviation are decisive factors to decrease the emittance and increase the final selectivity.

## V. ACKNOWLEDGEMENTS

Thanks to PEMM-COPPE-UFRJ and DIMAT-INMETRO-XERÉM for help in the experiments, to CNPq-Brazil for financial support and to Calouste Gulbenkian Foundation for grant process number 104299.

## VI. REFERENCES

- [1] A. R. Shashikala, A. K. Sharma, D. R. Bhandari, Solar selective black nickel–cobalt coatings on aluminum alloys, *Sol. Energy Mater. Sol. Cells*, vol. 91, 2007, pp. 629-635.
- [2] C.E. Kennedy, Review of Mid- to High-Temperature Solar Selective Absorber Materials, NREL National Renewable Energy Laboratory, 2002.
- [3] M. Thirugnanasambandam, S. Iniyan, R. Goic, A review of solar thermal technologies, *Renewable Sustainable Energy, Rev.* 1, 2010, pp. 312-322.
- [4] M. J. Atkins, M. R.W. Walmsley, A. S. Morrison, Integration of solar thermal for improved energy efficiency in low-temperature-pinch industrial processes, *Energy*, 2009, doi: 10.1016/j.energy.2009.06.039.
- [5] A. C. Oliveira, The energy shift: towards a renewable future, *Int. J. Low Carbon Technol.* 2, 2007, pp. 289-299.
- [6] Z. Sen, Solar Energy Fundamentals and Modeling Techniques: Atmosphere, Environment, Climate Change and Renewable Energy, © 2008 Springer-Verlag London Limited.
- [7] T. Tsoutsos, V. Gekas, K. Marketaki, Technical and economical evaluation of solar thermal power generation, *Renewable Energy*, vol. 6, 2003, pp. 873-886.
- [8] M. A. M. Ibrahim, Black nickel electrodeposition from a modified Watts bath, *J. Appl. Electrochem.*, vol. 36, 2006, pp. 295-301.
- [9] I. Gurrappa, L. Binder, Electrodeposition of nanostructured coatings and theircharacterization - a review, *Sci. Technol. Adv. Mater.*, vol. 9, 2008, pp. 043001.
- [10] The Copper Tube Handbook, Copper Development Association, Publishers, (Inc), New York, 2006.
- [11] J. K. Dennis, T. E. Such, in: Nickel chromium plating, Butterworth & Co.(Publishers) Ltda, London, 1972, Ch. 4 and 5.
- [12] K. S. Indira, S. R. Rajagopalan, M. I. A. Siddiqi, K. S. G. Doss, Black nickel plating, *Electrochim. Acta*, vol. 9, 1964, pp. 1301-1317.
- [13] W. Sade, R. A. X. Nunes, J. R. T. Branco, Deposição Química de Filmes de Ni/NiO em Substrato de Alumínio, *Metalurgia & Materiais*, vol. 62, 2009, pp. 361-365.
- [14] P. A. Galione, et al., *Surf. Coat. Technol.*, 2009), oi: 10.1016/j.surfcoat.2009.12.008.
- [15] R. D. Armstrong, J. A. Harrison, Two-Dimensional Nucleation in Electrococrystallization, *J. Eletrochem. Soc.*, 1969, pp. 328-340.
- [16] C. Gnecco, R. Mariano, F. Fernandes, Tratamento de Superficie e Pintura, Instituto Brasileiro de Siderurgia/ Centro Brasileiro de Construção em Aço, IBS/CSBCA, Rio de Janeiro, 2003, Ch. 1.
- [17] S. C. Chang, Y. L. Wang, Effects of applied voltages on planarization efficiency of Cu electropolishing, *J. Vac. Sci. Technol. B* 22, 2004, pp. 2754-2757.
- [18] R. L. P. Teixeira, L. Raniero, R. A. Simão, B. Coelho, Oliveira, A.C., Temperature influence on the thermal and structural properties of electrodeposited nanostructured black nickel's cermet on high conductive C81100 copper, *Int. J. Low-Carbon Tech. Low Carbon*, vol. 6, 2011.
- [19] Z. X. Wen, N. X. Hou, Z. F. Yue, Creep damage and crack initiation behaviour of nickel-base single crystalline superalloys compact tension specimen with a void ahead of crack tip, *Mater. Sci. Eng.,vol. A* 510-511, 2009, pp. 284-288.
- [20] W. M. Yin, S. H. Whang, R. Mirshams, C. H. Xiao, Creep behavior of nanocrystalline nickel at 290 and 373 K, *Mater. Sci. Eng., vol. A* 301, 2001, pp. 18-22.
- [21] J. R. Ares, A. Pascual, I. J. Ferrer, C. Sánchez, A methodology to reduce error sources in the determination of thin film chemical composition by EDAX, *Thin Solid Films*, vol. 1, 2004, pp. 207-210.
- [22] R. L. P. Teixeira, G. C. D. Godoy, M. M. Pereira; Calcium phosphate formation on alkali-treated titanium alloy and stainless steel. *Mater. Res.*, vol. 7, 2004, pp. 299-303.
- [23] X. Liu, U. Meridor, P. Zhao, G. Song, A. Frydman, A. Gedanken, The synthesis and magnetic properties of monodispersed single-domain nickel nanospheres and highly globular nanostructures of NicoreNiOshell, *J MAGN MAGN MATER*, vol. 301, 2006, pp. 13-21.

[24] X. Liu, X. Cai, J. Mao, C. Jin; ZnS/Ag/ZnS nano-multilayer films for transparent electrodes in flat display application, *Appl. Surf. Sci.*, vol. 183, 2001, pp. 103-110.

[25] J. Chen, Chen. Li, J.L. Song, X.W. Sun, W. Lei, W.Q. Deng, Bilayer ZnO nanostructure fabricated by chemical bath and its application in quantum dot sensitized solar cell, *APPL SURF SCI* 255, 2009, pp. 7508-7511.

[26] Ali Moghani, Study of Symmetries on some Chemical Nanostructure, *J NANO RES-SW*, vol. 11, 2010, pp. 7-11.

Ricardo Luiz Perez Teixeira  
Programa de Engenharia Metalúrgica e de Materiais, PEMM-COPPE  
Universidade Federal do Rio de Janeiro  
Cid. Universitária-Centro de Tecnologia-Bloco F, sala F-210, Ilha do Fundão  
- Caixa Postal 68505; CEP 21941-972, RJ, Rio de Janeiro  
BRAZIL  
[rlpteixeira@metalmat.ufrj.br](mailto:rlpteixeira@metalmat.ufrj.br), [ext09079@fe.up.pt](mailto:ext09079@fe.up.pt)  
<http://www.metalmat.ufrj.br>

Renata Antoun Simão  
Programa de Engenharia Metalúrgica e de Materiais, PEMM-COPPE  
Universidade Federal do Rio de Janeiro  
Cid. Universitária-Centro de Tecnologia-Bloco F, sala F-210, Ilha do Fundão  
- Caixa Postal 68505; CEP 21941-972, RJ, Rio de Janeiro  
BRAZIL  
[renata@metalmat.ufrj.br](mailto:renata@metalmat.ufrj.br) <http://www.metalmat.ufrj.br>

Bruno Coelho  
IDMEC - New Energy Technologies Unit  
Faculty of Engineering, University of Porto  
Rua Dr. Roberto Frias, CEP, 4200-465, Porto  
PORTUGAL  
[bcoelho@fe.up.pt](mailto:bcoelho@fe.up.pt)  
<http://www.fe.up.pt/idmec/net/>

Armando Coelho Oliveira  
IDMEC - New Energy Technologies Unit  
Faculty of Engineering, University of Porto  
Rua Dr. Roberto Frias, CEP, 4200-465, Porto  
PORTUGAL  
[acoliv@fe.up.pt](mailto:acoliv@fe.up.pt)  
<http://www.fe.up.pt/idmec/net/>